Shape of the yumi

John C. Neu

August 13, 2019

From the strictly mechanical point of veiw, a yumi is a thin elastic rod. Our analysis of yumi statics idealizes it as a material plane curve with a specified variation of stiffness along its length. The in-plane assumption is of course not exact for real yumi, so we are working in a (conscious) approximation. Let $\mathbf{x}(s)$ be the displacement vector from the lower tip to the point on the yumi at arclength s from the bottom. The unit tangent to the curve at $\mathbf{x}(s)$ is

$$\mathbf{t}(s) := \dot{\mathbf{x}}(s). \tag{1}$$

The tangent is oriented in the direction, from the lower to upper tip. Let $\theta(s)$ denote the angle of the tangent $\mathbf{t}(s)$ relative to a fixed direction ("positive horizontal"). The *curvature* of the yumi at $\mathbf{x}(s)$ is defined as $\dot{\theta}(s)$. Figure 1 is the visuualization of these defintions for a braced yumi. Short segments of yumi about $\mathbf{x}(s)$ are closely approximated by a circle of radius $1/|\dot{\theta}(s)|$ which "kisses" the yumi at $\mathbf{x}(s)$. This captures the geometric meaning of the curvature's *magnitude*. In general, curvature may be positive or negative. In figure 1, notice that the curvature is *positive* along segments of yumi which are *convex* when veiwed from the belly, and *negative* for segments which are *concave*.

Braced yumi

For a braced yumi, the tsuru connects the bottom and top tips by a straight line. Letting L_s denote the length of tsuru, we have

$$L_s = |\mathbf{x}(L)|. \tag{2}$$

Here, we have

$$\mathbf{x}(L) = \int_0^L \mathbf{t}(s) ds, \tag{3}$$

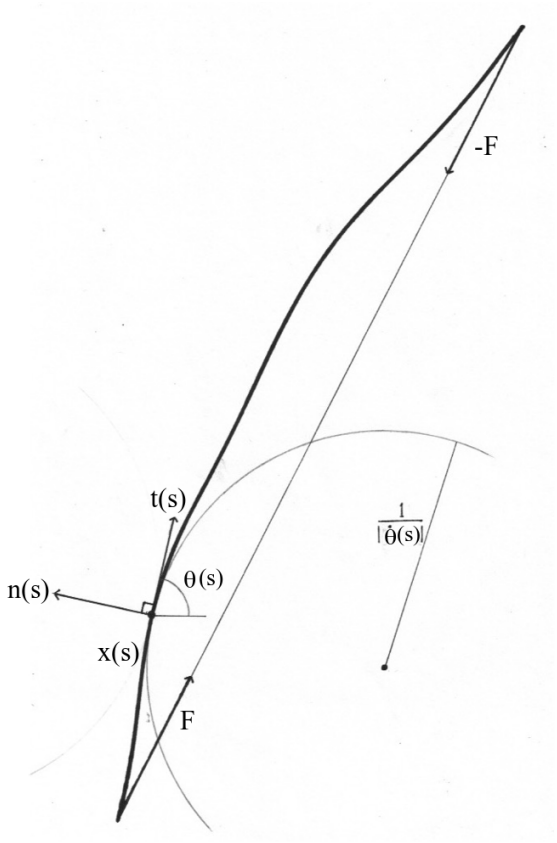

Figure 1

where L is the total arclength of yumi. (3) follows by integration of (1) from $s = 0$ to $s = L$. (2) amounts to a *contraint* on possible braced yumi configurations. Since any two configurations related by a translation and a solid body rotation in the plane are physically equivalent, we can fix $\mathbf{x}(L)$ to *one given point* $\mathbf{X}$ on the circle of radius L_s. Hence, we'll work with the constraint

$$\mathbf{x}(L) = \int_0^L \mathbf{t}(s)ds = \mathbf{X} = given, \tag{4}$$

The physical principle which determines the shape of the bow between given endpoints $\mathbf{x} = 0$ and $\mathbf{x} = \mathbf{X}$ is *energy minimization*: Let $\kappa(s)$ be the

curvature of the unbraced bow as a function of arclength s. The *curvature difference* $\dot{\theta}(s) - \kappa(s)$ between braced and unbraced configuations represents actual physical bending which has an energy cost. The elastic energy per unit length is proportional to $(\dot{\theta}(s) - \kappa(s))^2$. This proportionality is elaborated in Landau and Lifshitz "Theory of Elasticity." Details aside, energy per unit length proportional to the square of curvatuve change is intuitively plausible. Its the usual quadratic variation of a function due to small displacements from its minimum. The *elastic energy* stored in the whole bow is

$$E = \frac{1}{2}\int_0^L \mu(s)(\dot{\theta}(s) - \kappa(s))^2 ds. \tag{5}$$

Here, $\mu(s)$ is the *bending modulus* along the length of the bow. It is specified by materials and tapering. Here, we assume it is given. We seek the configuration $\theta = \theta(s)$ which minimizes the energy E subject to the constraint (4). It is sufficient to consider the modified energy

$$\bar{E} := E + \mathbf{F} \cdot (\mathbf{x}(L) - \mathbf{X}), \tag{6}$$

where $\mathbf{F}$ is a two-vector of Lagrange multipliers. Using (3), we may reformulate the modified energy (6) as

$$\bar{E} = \int_0^L \{\frac{\mu}{2}(\dot{\theta} - \kappa)^2 + \mathbf{F} \cdot \mathbf{t}\} ds - \mathbf{F} \cdot \mathbf{X}\ L. \tag{7}$$

The variation of this energy due to variation $\delta\theta$ of θ is

$$\begin{aligned} \delta\bar{E} = \quad & \int_0^L \{\mu(\dot{\theta} - \kappa)\delta\dot{\theta} - \mathbf{F} \cdot \mathbf{n}\ \delta\theta\} ds = \\ & [\mu\ (\dot{\theta} - \kappa)\ \delta\theta]_0^L + \int_0^L \{-\frac{d}{ds}(\mu(\dot{\theta} - \kappa)) + \mathbf{F} \cdot \mathbf{n}\}\ \delta\theta\ ds. \end{aligned} \tag{8}$$

Here, $\mathbf{n}$ is the unit normal of the yumi curve, oriented so $\mathbf{t}$ and $\mathbf{n}$ are a right-handed pair, as in figure 1. We used $\delta\ \mathbf{t} = \mathbf{n}\ \delta\theta$. The vanishing of $\delta\bar{E}$ for all $\delta\theta$ leads to the *elastic boundary value problem* for $\theta(s)$,

$$\frac{d}{ds}(\mu(\dot{\theta} - \kappa)) - \mathbf{F} \cdot \mathbf{n} = 0,\ 0 < s < L, \tag{9}$$

$$\dot{\theta} = \kappa,\ s = 0, L. \tag{10}$$

The boundary conditions (10) express *no bending at the ends.* The two-vector $\mathbf{F}$ of Lagrange multipliers is presumably chosen so the bow shape defined by the solution of (9) and (10) achieves the end to end displacement in (4).

Tsuru tension

Integration of (9) over $0 < s < L$ and use of boundary conditions (10) gives

$$\mathbf{F} \cdot \int_0^L \mathbf{n} ds = 0. \tag{11}$$

Notice that $\mathbf{n} = J\mathbf{t}$, where J represents counterclockwise rotation of $\pi/2$ radians. Hence

$$\int_0^L \mathbf{n} ds = J \int_0^L \mathbf{t} ds = J\mathbf{X}.$$

The last equality uses (4). Hence (11) reduces to $\mathbf{F} \cdot J\mathbf{X} = 0$, which says that the two-vector of Lagrange multipliers is *proportional* to $\mathbf{X}$. In the modified energy (6), it is evident that $\mathbf{F}$ has the units of *force* and its proportionality to the end to end displacement suggests its physical meaning is *tsuru tension.* This is clearer when we contemplate the physical meaning of the component

$$U := \mathbf{F} \cdot (\mathbf{x}(L) - \mathbf{X}) \tag{12}$$

of the modified energy (6). Formally, U can be regarded as the potential energy of a particle in a uniform force field $-\mathbf{F}$ at position $\mathbf{x}(L)$. So: the string is exerting tension $-\mathbf{F}$ at the upper tip.

Intuitively, the tsuru tension acting on the upper tip should point to the lower tip, so $-\mathbf{F}$ is in the direction opposite $\mathbf{X}$. Equivalently, $\mathbf{F}$ is parallel to $\mathbf{X}$. The tsuru exerts tension $\mathbf{F}$ on the lower tip. The tension forces are displayed in figure 1. We outline a plausibility argument for $\mathbf{F}$ parallel to $\mathbf{X}$ when the unbraced curvature profile $\kappa(s)$ is sufficiently small in magnitude. Adopt cartesian x, y coordinates with the origin at the lower tip, and the upper tip is at $(X, 0)$ with $X > 0$. Then $\mathbf{F} = F\hat{\mathbf{x}}$, and we are to show $F > 0$. The normal $\mathbf{n}(s)$ has coordinate representation $\mathbf{n}(s) = -\sin\theta(s)\hat{\mathbf{x}} + \cos\theta(s)\hat{\mathbf{y}}$, so $\mathbf{F} \cdot \mathbf{n} = -F\sin\theta(s)$ and the ODE (9) reads

$$\frac{d}{ds}(\mu(\dot{\theta} - \kappa)) + F\sin\theta = 0. \tag{13}$$

Multiplying (13) by $\sin\theta$, integrating over $0 < s < L$ and use of the boundary conditions (10) gives

$$\int_0^L \mu\cos\theta(\dot{\theta} - \kappa)^2 ds + \int_0^L \mu\kappa\cos\theta\,(\dot{\theta} - \kappa) ds = F\int_0^L \sin^2\theta\, ds. \tag{14}$$

Take $\kappa(s) \equiv 0$, corresponding to an unbraced yumi with *no* curves. That is, a straight line. Then (14) reduces to

$$\int_0^L \mu \cos\theta \, \dot{\theta}^2 ds = F \int_0^L \sin^2\theta \, ds. \tag{15}$$

Assuming that the length of the tsuru is less than the length of the yumi, the braced shape is a convex curve with endpoints at $(0, 0)$ and $(X, 0)$, depicted in figure 2. We anticipate $\theta(s)$ and $\dot{\theta}(s)$ not identically zero, with $|\theta(s)| < \pi/2$

Figure 2

(no vertical tangents). Then the integrals in the LHS and RHS of (15) are both positive, so F must be positive as well.

Lets now introduce *nonzero* unbraced curvature $\kappa(s)$. If its magnitude in $0 < s < L$ is sufficiently small,, the integrals on the LHS and RHS of (14) remain positive (we appeal to continuity), and F remains positive.

Is F positive for *all* profiles $\mu(s) > 0$ and $\kappa(s)$? Well, no. Suppose the unbraced shape is like figure 2, but the endpoints are close together than the prescribed value X. Then the constraint force needs to pry the ends apart, as depicted in figure 3, and we have $F < 0$.

Figure 3

Torque identity

Integration of (9) from $s = 0$ to any s between 0 and L and use of the boundary condition at $s = 0$ gives the identity

$$(\mu(\dot{\theta} - \kappa))(s) = \mathbf{F} \cdot J\mathbf{x}(s). \tag{16}$$

Here, we used

$$\int_0^s \mathbf{n}(s')ds' = J \int_0^s \mathbf{t}(s')ds' = J\mathbf{x}(s).$$

Let us introduce cartesian axes as before, with the lower tip of yumi at the origin, and the upper tip at $(X, 0)$. The tsuru occupies the x-axis between $x = 0$ and $x = X$. The yumi is expected to lie above the x-axis, with elevation $y(s) > 0$ at $\mathbf{x}(s)$. Figure 4 visualizes this geometry and its coordinate description. In this coordinate description, we have $\mathbf{F} \cdot J\mathbf{x}(s) = -Fy(s)$, and (16) reads

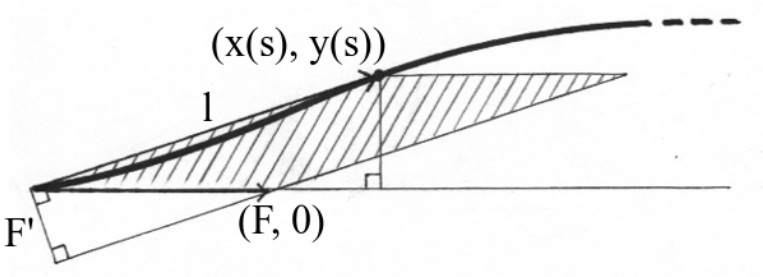

Figure 4

$$(\mu \Delta\kappa)(s) = -Fy(s). \tag{17}$$

Here,

$$(\Delta\kappa)(s) := (\dot{\theta} - \kappa)(s) \tag{18}$$

Geometrically, the $Fy(s)$ is the area of the parallelogram spanned by $\mathbf{F}$ and $\mathbf{x}(s)$: Regarding $\mathbf{F}$ as the base, $y(s)$ is the height and we have area = base $\times$ height $= Fy(s)$. Alternatively, take $\mathbf{x}(s)$ as the base. Let l denote its length. The height is F', the length of $\mathbf{F}$'s projection onto a line perpendicular to $\mathbf{x}(s)$. The area is also represented as $F'l$.

Physically, $-Fy(s) = -F'l$ is the *torque* exerted by the tsuru tension on the limb at $\mathbf{x}(s)$. The minus sign in (18) indicates that this torque acts in a counterclockwise sense. It induces a bending at $\mathbf{x}(s)$ which is convex when seen from the back ($\dot{\theta} - \kappa < 0$). We refer to (17) as the *torque identity*.

Roles of the torque identity in measurement and design

In principle, the torque identity allows the determination of the modulus profile $\mu(s)$ from a comparison of unbraced and braced yumi shapes and measurement of the tsuru tension F. The unbraced configuration specifies the unbraced curvature $\kappa(s)$. The braced configuration specifies the elevation, angle and curvature profiles $y(s)$, $\theta(s)$, $\dot{\theta}(s)$, and the tsuru tension F. The

bending modulus profile now follows by a *calculation*,

$$\mu(s) = \frac{Fy(s)}{\Delta\kappa(s)}. \tag{19}$$

We forsee a role of the torque identity in *design*. The prefered shape of the braced yumi is a strong focus of cultural aesthetics. The yumishi has a strong sense of what the braced yumi *should* look like, and the question for the yumishi is: What unbraced shape should be laminated in order to achieve the chosen braced shape? In particular: How to achieve the proper gap between the tsusru and the upper strike plate for good tsurune? In the conventional physics perspective, the "knowns" are the profiles of bending modulus and unbraced curvature, and the *forward* problem is to solve the elastic boundary value problem (9), (10) for the braced shape and tsuru tension. The yumishi needs to solve the *inverse problem*: Find the unbraced shape from the braced. His mathematical calculation is much simpler than the forward problem. For the moment, let us take the modulus profile $\mu(s)$ as *given*, prescibed by conventional tapering of yumi limbs in both thickness and width. The torque identity (an *integral* of the elastic boundary value problem) specifies the unbraced curvature profile $\kappa(s)$ from the braced curvature and elevation profiles $\dot{\theta}(s)$ and $y(s)$, with the tsuru tension F as a parameter. We see that the yumishi calculates not one unique unbraced shape, but rather a *family* of candidate shapes with different tsuru tensions F. The ura-zori of each candidate shape is specified by the tsuru tension F. In general, we achieve higher tsuru tension by increasing ura-zori. In practice, the yumishi selects an unbraced shape with ura-zori in the conventional range, $15cm - 20cm$, since yumi with too much ura-zori are prone to flipping when shot. There is a lot of physics behind this short preview. We bcome back to it when we know more.

Mapping stiffness profiles

The program is to estimate the bending modulus profile of actual yumi by inputing measured values of tsuru tension F, elevation profile $y(s)$ and curvature change profile $\Delta\kappa(s)$ into (19). Measurements of the tsuru tension and elevation profile are straightforward. The first panel of figure 5 depicts a yumi braced with a "measurement" tsuru, consisting of two segments of steel cable with a turnbuckle length adjuster and digital scale interpolated in between. The second panel is a close-up of the turnbuckle and scale. When a time dependent force is exerted on the scale, it records the *maximum* force

achieved during its application. With a little practice of bracing the yumi with the measurement tsuru, the recorded tension is in fact the static tension F, reproducable in repeated trials. To measure the elevation profile, replace the measurement tsuru by a regular tsuru adjusted to the same brace height. The regular tsuru presents an unobstructed straight line. The elevation of the yumi center-line above the tsuru is measured in *cm* with a standard archery T-square, as depicted in the third panel of figure 5.

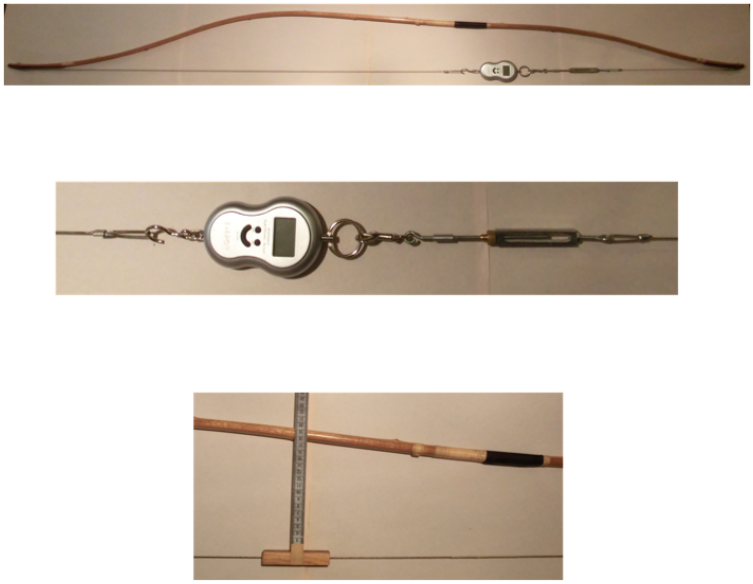

Figure 5

Measurement of the curvature change profile $\Delta\kappa(s)$ is much more difficult. Estimating mathematical derivitives from noisy data is *not* an experimentalist's favorite proceedure. Curvature is in essence a *second* derivitive and the bamboo surfaces of a yumi are obviously "noisy." Look at the center-axis of the back: It is close to but not exactly a plane curve, and it has a "rough topography" due to natural features such as the nodal ridges. The mathematical curvature of this center-axis for both unbraced and braced yumi has large fluctuations reflecting this roughness. Fortunately, the effects of this roughness nearly cancel when we examine the *change* in curvature induced by bracing. A "geodesy" visualization helps: Imagine the intersection between a plane of fixed latitude and the surface of the earth as we transect the Himalaya. In figure 6, the smooth arc represents "sea level" and the jagged

solid curve, the rough topography of the Himalaya along the line of latitude. Imagine three surveyors at points $a,\ b,\ c$. They can measure the elevation of the line ac as it passes over b. Let $a',\ b',\ c'$ be projections of $a,\ b,\ c$ down to sea level. Notice that b' is above the line $a'c'$. Later, the curve representing sea level changes due to the movement of the moon. The elevation of b' above the line $a'c'$ changes, reflecting a change in curvature of the sea level arc. assuming that the elevations of $a,\ b,\ c$ relative to $a',\ b',\ c'$ remain fixed, the elevation of b relative to the line ac as it passes overhead changes by essentially the same amount. Hence, the surveyors on the rough Himalaya topography can estimate the distortion of the sea level arc. The change in elevation of b relative to the line ac as it passes overhead is proportional to the change in curvature.

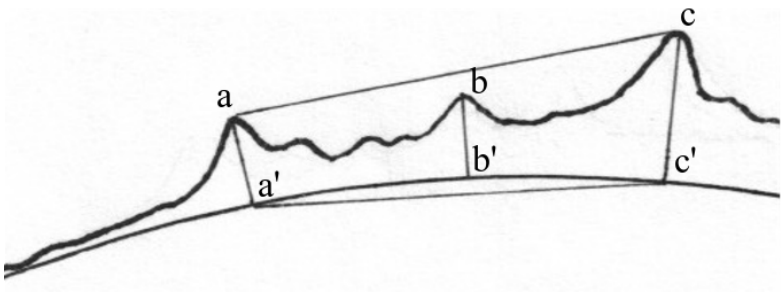

Figure 6

Figure 7 depicts the jig which carries out this "geodesy exercise" on the back of a yumi. The jig contacts the yumi's back at three points. Two "right feet" touch down on either side of the center-axis. A prong in between the feet aids centering. The left foot is a spring-loaded screw. The three contact points define a plane, and we measure the elevation of the yumi's back at the halfway mark between the left and right feet, relative to this plane. This is the job of the depth gauge. For instance, suppose the elevation is positive. We "zero" the jig by placing it on a (really) flat surface and turning the spring-loaded screw on the left so the depth gauge plunger just touches the reference flat. Now carefully plant the feet of the jig on a section of yumi back as described before. The depth gauge records a deflection of the plunger in *mills*. (one mill equals one one thousandth of an inch.) If the elevation is negative, we first place the jig on the yumi's back and turn the screw until the depth gauge plunger just touches the yumi. We then place the jig on the reference flat and record the deflection. As in the geodesy example,

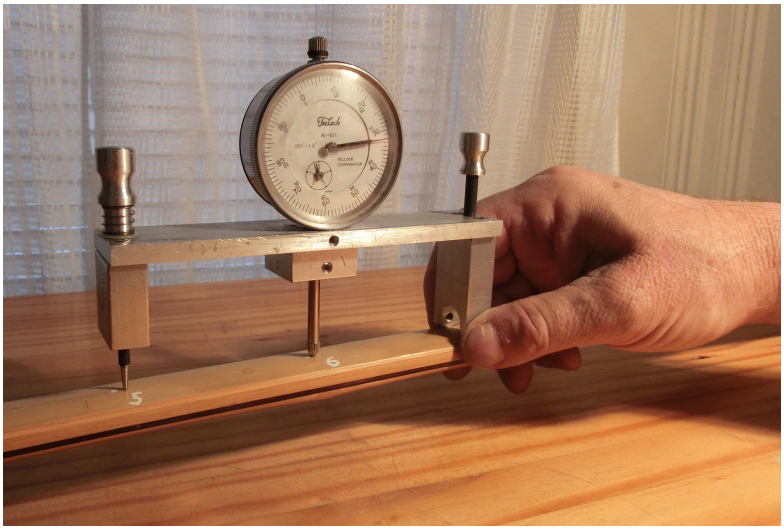

Figure 7

the change in curvature induced by bracing the yumi is proportional to the change in the elevation. the conversion from elevation change to curvature change is $.00974m^{-1}$ of curvature change for each mill of elevation change.

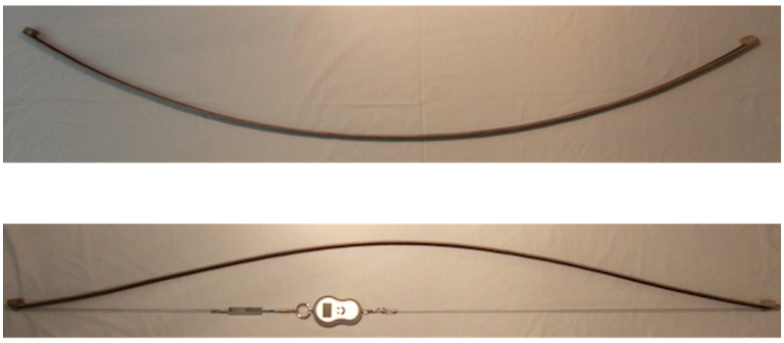

Figure 8

We present results of measurements. We begin with a simple test of the torque identity. A laminated beam is constructed: It is depicted in the first panel of figure 8. Carbon skins analogous to the bamboo back and belly of a yumi are separated by an oak core made of two layers: The core layers are "book-matched" so their tendencies for out of plane twist cancel. The cross section has a width of $2.9cm$ and a total thickness of $3.9mm$. Each carbon

skin is $.4mm$ thick. The beam with a total length of $L \approx 183cm$ is layed up into an arc of a circle whose radius equals the length L. The second panel of figure 8 depicts the braced beam, analogous to the braced yumi depicted in figure 5. The measured tsuru tension is $F \approx 7.67kg$. The elevation profile and curvature change induced by bracing are measured at six points along the center axis of the beam's back, starting from, the center and proceeding to one end in $16cm$ increments. These measurements are recorded in table 1. The last column records estimates of bending modulus based upon the torque identity. The beam is fabricated to have nominally uniform cross section and

Table 1: Test of torque identity

$y\ (cm)$	$\Delta\kappa\ (m^{-1})$	$\mu\ (kg\ m^2)$
22.2	-1.40	1.21
21.2	-1.32	1.23
18.0	-1.15	1.20
13.1	-.84	1.19
8.2	-.39	1.29
3.2	-.21	1.19

hence uniform modulus. The moduli in table 1 have mean value 1.22 $kg\ m^2$ with 7% root mean square variation.

We carry out a similiar program for two Yonsun yumi of yumishi Don Symanski. The first, crafted in '06, is an "old favorite" over many years of practice. It has a low ura-zori of $10cm$. The second, crafted in '18 has a robust ura-zori of $17cm$. The tsuru tensions of both yumi are measured at the standard $15cm$ brace height, $30.8kg$ for the '06 yumi, $30.5kg$ for the '18 yumi. Measurement points where the depth gauge plunger contacts the back of the yumi are placed in specific relation to the nodes: There are measurement points directly above belly nodes. There are measurement points close to the middle of segments whose endpoints are one belly node and one back node. Care is taken so the jig's contact points don't land directly on top of a back node's ridge. Finally, there are measurement points almost on top of a back node. The back nodes usually have a relatively flat "shelf" adjacent to the sharp ridge, which is the best "landing point" for the depth gauge plunger. The grip and rattan above the grip are stripped, to get good

contact points for the feet of the jig for measurement points near the grip. For each measurement point, we record the arclength from the top of the grip in *cm*, the elevation of the yumi's neutral axis above the tsuru in *cm*, and the curvature change induced by bracing, in m^{-1}. From the measured values of tsuru tension, elevation, and curvature change we calculate bending moduli from the torque identity (19). Figure 9 displays the experimentally determined modulus profiles of the '06 and '18 yumi. The horizotal axes are arclength from the top of the grip, positive above and negative below. The vertical axes are bending modulus. Squares represent measurement points at nodes, circles, measurement points between nodes.

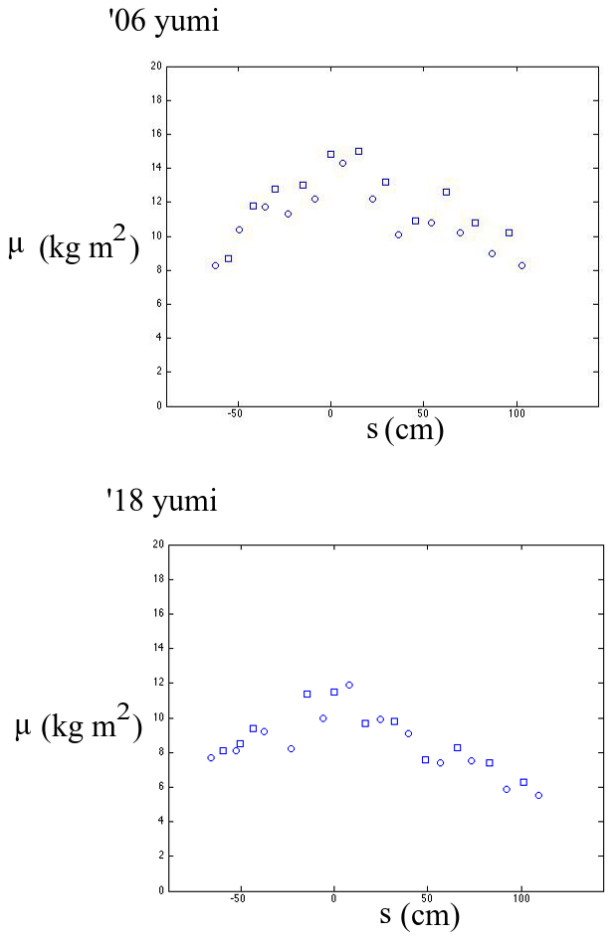

Figure 9

The simplest bow

Figure 10 depicts a "cartoon" bow in its unbraced and braced configurations. Its stiffness and unbraced curvature are *uniform* over its length: μ, κ are positive constants. Geometrically, the unbraced bow is an arc of a circle, *concave* when veiwed from the back. The distance from the midpoint of the unbraced bow to the line between the tips is called the *reverse height*, analogous to the "ura-zori" of the unbraced yumi. We nondimensionalize the elastic boundary value problem for the angle profile $\theta(s)$ based on the units $[s] = L, [F] = \mu/L^2$. The dimensionless equations are

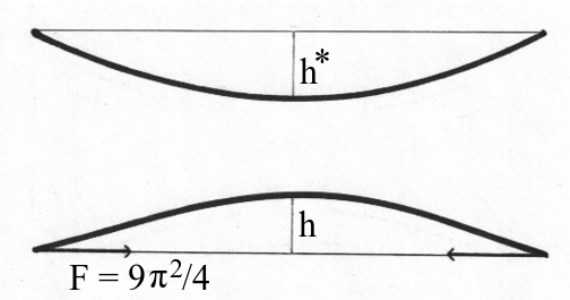

Figure 10

$$\ddot{\theta} + F \sin\theta = 0,\ 0 < s < 1, \tag{20}$$

$$\dot{\theta} = \epsilon := \kappa L,\ s = 0, 1. \tag{21}$$

We assume small *reflex* in the sense that $\epsilon := \kappa L << 1$. We further assume that the angle profile $\theta(s)$ of the braced bow is also small, so we approximate the ODE (20) by its linearization,

$$\ddot{\theta} + F\theta = 0,\ 0 < s < 1. \tag{22}$$

The analysis begins with the linearized ODE (22) subject to the boundary condition (21) with $\epsilon << 1$.

Braced longbow and Euler's column

For $\epsilon = 0$, the unbraced bow is straight and we'll call this case the "longbow." We have an "archery" version of the famous Euler column buckling: (22) subject to zero boundary conditions at the tips is an eigenvalue problem with the dimensionless string tension F as the eigenvalue. The smallest positive eigenvalue is $F = \pi^2$, representing the minimum tension required

to sustain a bending of the bow. The dimensional version of this minimum tension is

$$F = \pi^2 \frac{\mu}{L^2} \tag{23}$$

The corresponding angle profile $\theta(s)$ is a multiple of the eigenfunction $\cos(\pi s)$. That is,

$$\theta(s) = \pi h \cos(\pi s), \tag{24}$$

where h is a constant. From the angle profile we recover the braced bow configuration as a curve in the x, y plane parametrized by arclength. The parametric equations are

$$x = x(s) = \int_0^s \cos\ \theta(s')ds',\ y = y(s) = \int_0^s \sin\ \theta(s')ds'. \tag{25}$$

Under the small angle approximation, (25) asymptotically reduces to

$$x \sim s,\ y(s) \sim \int_0^s \theta(s')ds'. \tag{26}$$

Substituting (24) for $\theta(s)$, we deduce from (26),

$$y(s) \sim h \sin(\pi s),\ 0 < s < 1. \tag{27}$$

Since $s \sim x$ as in (26), we have the *Monge representation* (That is, y as a function of x) of bow shape,

$$y = y(x) \sim h \sin(\pi x),\ 0 < x < 1. \tag{28}$$

Figure 11 depicts the braced longbow, as a "half-period of a sine wave." All quantities in the labeling are dimensionless. We see that the constant $h > 0$ represents the *brace height*, the elevation of the bow above the string at the midpoint between the tips.

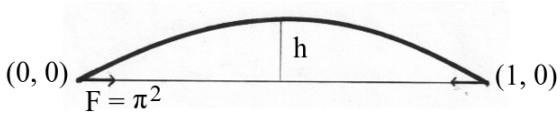

Figure 11

We discuss the apparent irrelevance of the remaining eigenvalues, $F = \pi^2 n^2$ for n an integer greater than one, and the associated eigenfunctions,

$\theta(s) \propto \cos(n\pi s)$. For instance, take $n = 2$, which would give a string tension $F = 4\pi^2$, *four* times that of the longbow. The corresponding shape of braced bow that follows from the angle profile $\theta(s) \propto \cos(2\pi s)$ is $y(x) \propto \sin(2\pi s)$. Figure 12 depicts the presumed physical situation. Aside from the string passing through the midpoint of the bow (you could make a slot in the beam, through its function as a bow remains questionable), the real issue is *no stability*. The configuration is a mechanical equilibrium, but any small perturbation away from it induces the beam to snap into one of the two stable configurations, analogous to the simple arc of the longbow (the thin curves in figure 12). Of course, the string tension recovers to the longbow value close to π^2. Are the $n > 1$ eigenpairs totally irelevant? Be advised! A ghost of the $n = 2$ eigenpair insinuates itself in the physics of the reflex bow with $\epsilon > 0$.

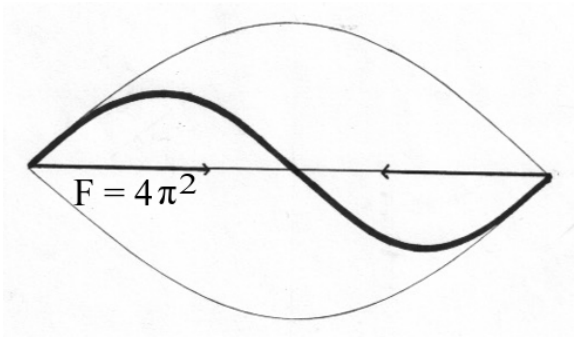

Figure 12

Reflex bow

We examine the effect of small positive reflex, $0 < \epsilon << 1$. The unbraced configuration depicted in figure 5 is a section of a circle of dimensionless radius $1/\epsilon$. By elementary trigonometry, we find that the dimensionless reverse height h^* is given by

$$h^* = \frac{1}{\epsilon}(1 - \cos(\frac{\epsilon}{2})) \sim \frac{\epsilon}{8}. \tag{29}$$

For $F \neq \pi^2 n^2$, $n =$ integer (the eigenvalues of longbow bending), the boundary value problem (21), (22) has the *unique* solution

$$\theta(s) = \frac{\epsilon}{\sqrt{F}\cos(\frac{\sqrt{F}}{2})} \sin(\sqrt{F}(s - \frac{1}{2})). \tag{30}$$

The nonuniform validity of (29) as F approaches one of the eigenvalues $\pi^2 n^2$ with n *odd* is obvious due to the vanishing of $\cos(\sqrt{F}/2)$ in the denominator. For $F = \pi^2 n^2$ with n *even*, the angle profile (29) is still a solution of (21), (22), but *not unique*. This simple mathematical fact induces a peculiar twist in the narrative of the physics. We'll come to that. The Monge representation of bow shape in the x, y plane based on the angle profile (30) is given by

$$y(x) \sim \frac{\epsilon}{F}\{1 - \frac{\cos(\sqrt{F}(x - \frac{1}{2}))}{\cos(\frac{\sqrt{F}}{2})}\}. \tag{31}$$

The *brace height* $h := y(1/2)$, the elevation of the bow's midpoint above the string, is given by

$$h \sim \frac{\epsilon}{F}\{1 - \frac{1}{\cos(\frac{\sqrt{F}}{2})}\}. \tag{32}$$

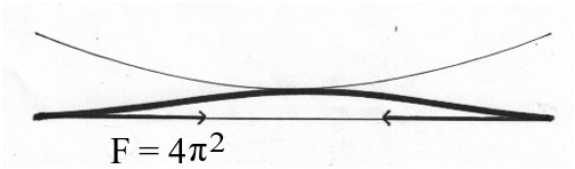

Figure 13

We concentrate on the (plausible) bow shapes for string tension in the range $\pi^2 < F < 4\pi^2$. In this range of tensions, $y(x) > 0$ in $0 < x < 1$ so the bow contacts the string only at the tips. As $F \to \pi^2$ from above, we deduce from (31), (32) that $y(x)$ is asymptotic to the longbow shape (28). In the limit $F \to \pi^2$ from above, h/ϵ in (32) diverges, so $h >> \epsilon$, but the asymptotic shape (28) still applies provided that h remains much less than unity. In summary, the asymptotic reduction to (28) applies for h in the intermediate range of magnitudes, $\epsilon << h << 1$. As F increases through the range $\pi^2 < F < 4\pi^2$, we obtain a sequence of shapes with *decreasing* brace heights. The shape depicted in figure 11 is based on (31) with $F = 9\pi^2/4$, which is 2.25 times the longbow tension. It has $h/h^* \approx .870$, so the brace height is a little bit less than the reverse height. As $F \to 4\pi^2$ from below, the shape asymptotes to

$$y(x) \sim \frac{\epsilon}{2\pi^2}\sin^2(\pi x),$$

depicted in figure 13. The arc marked by a light curve represents the unbraced shape. For this shape, the brace height is so low, $h/h^* \approx .405$, that the string is tangent to the bow at the tips. Recall that the tsuru of a yumi is almost tangent to the upper tip of the yumi.

Brace height versus string tension

Figure 14 is the graph of h/h^* versus F based upon (29), (32). The vertical asymptote at $F = \pi^2$ indicates that the small bending approximation is nonuniformly valid as $F \to \pi^2$ from above. We expect that (32) applies, so long as the brace height has the same order of magnitude as h^*. In this region

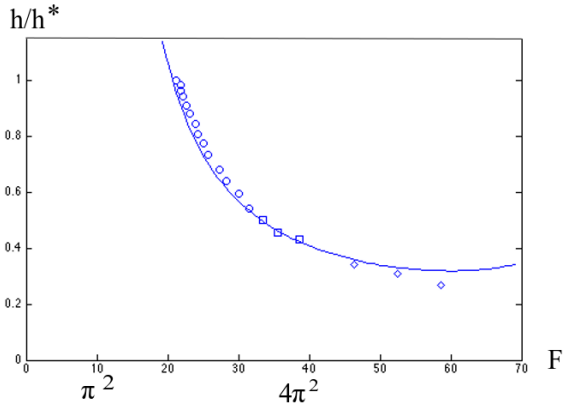

Figure 14

of the graph, we see that tension *increases* with *decreasing* brace height. This may appear counterintuitive: Shorten the string, raise the brace height, put the bow under more strain, yet the string tension required to maintain this more strained configuration is *less*, not more. The real understanding is informed by the torque identity (17). In figure 4, take the point $(x(s), y(s))$ to be the midpoint of the bow, so $y(s) = y(1/2) = h$, the brace height. Look at the torque exerted on the midpoint of the bow by the string tension acting on the lower tip. The magnitude of this torque is the area Fh of the parallelogram. According to the torque identity, the induced change $\Delta\kappa$ in curvature at the midpoint from the unbraced configuration is

$$\Delta\kappa = -\frac{Fh}{\mu}. \tag{33}$$

This minus sign indicates bending which is concave *down*. The dimensionless version based on the units $[h] = L$, $[\Delta\kappa] = 1/L$, $[F] = \mu/L^2$ is (33) with μ

set to unity. For the angle profiles in (30), we calculate

$$\Delta\kappa = \dot{\theta}(\frac{1}{2}) - \epsilon = \frac{\epsilon}{\cos(\frac{\sqrt{F}}{2})} - \epsilon,$$

and substitution into (the dimensionless version of) (33) gives

$$\epsilon\{1 - \frac{1}{\cos(\frac{\sqrt{F}}{2})}\} = Fh,$$

which reproduces (32), the basis of the graph in figure 14. In summary, (32) *is* the torque identity applied to the bending of the bow at its midpoint. An intuition: As the brace height increases, the string tension has more leverage to bend the bow at its midpoint, and the required string tension decreases.

The increase of string tension as the string lengthens and the brace height decreases is a striking prediction which may be tested by physical measurements. Our first experiment employs the carbon-skinned beam depicted in figure 5 with nominally uniform curvature and bending modulus. Since the beam is close to a circular arc whose radius is the same as the beam length $L \approx 183cm$, the dimensionless curvature is $\epsilon \approx 1$, which doesn't seem especially small. This is a pragmatic choice: If the reverse height is too small relative to the total length, the actual physical experiment is highly sensitive to small changes in string length. We employ a "measurement" string analogous to the one depicted in figure 5, with interpolated digital scale and turnbuckle length adjustment. In fact, the second panel of figure 8 shows the beam braced with the measurement string.

The obvious experiment is to vary the string length with the turnbuckle, and for each fixed string length, record the brace height h and static string tension F. Table 2 depicts a typical data set. The first column records the brace height in cm, and the third, the string tension in kg. Each of the braced configurations is symmetric about the midpoint of the beam (the second panel of figure 8 depicts a typical example), and physically stable. The increase of string tension with decreasing brace height is obvious. For contemplating the relevance to yumi, it is helpful to compare the brace height to the reverse height h^*, whose measured value is $22.5cm$. The second column of table 2 records brace heights in units of this reverse height. Recall that the nominal brace heigth of yumi is $15cm$, and the nominal ura-zori has reverse height in the nominal range of $15 - 20cm$. We see that the nominal range of

Table 2: Brace height versus string tension

$h\ (cm)$	h/h^*	$F\ (kg)$	$F/(\mu/L^2)$
22.5	1.00	7.63	21.2
22.15	.984	7.86	21.8
21.7	.964	7.90	21.9
21.2	.942	7.96	22.1
20.5	.911	8.17	22.6
19.9	.884	8.38	23.2
19.05	.847	8.65	24.0
18.15	.807	8.75	24.3
17.45	776	9,06	25.1
16.5	.733	9.30	25.8
15.3	.680	9.85	27.3
14.4	.640	10.20	28.3
13.4	.596	10.84	30.0
12.2	.542	11.34	31.5

brace height in units of reverse height is $.75 - 1.0$, which is included in the range of values in table 2.

A quantitative comparison between the measured relation between brace height and string tension and the theoretical relation (32) requires an additional piece of information *not* included in the raw data, of h in cm versus F in kg. In (31), string tension is measured in units of μ/L^2. The beam length is known, $L \approx 183cm$, but we need to input the bending modulus μ. One approach is to *choose* μ so the theoretical curve based upon (32) fits the data in a least squares sense, such as minimizing the sum of squared differences between measured and theoretical values of h for each value of F in table 2. we don't do this: Such a fit can mask systematic departures from the linearized theory which is the basis of (32). A more direct method is to use the average of the bending modulii in table 1, $1.22kg\ m^2$, which we determined in the earlier test of the torque identity. Given this estimate of bending modulus, and beam length $L \approx 183cm$, we find that the scaling unit μ/L^2 of string tension is $.364kg$. The fourth column of table 1 lists the dimensionless string tensions. The circles in figure 14 represent of sequence of

points in the plane whose axes are $h/h^{*}*$ and F. The systematic discrepancy between the data and the simple linearized $\epsilon \to 0$ theory is not so surprising: ϵ is actually close to 1. The real lesson behind the data of table 1 is the *range* of measured string tensions. Recall that the "longbow" string tension obtained by bracing a beam with no reverse height is $F = \pi^2\mu/L^2$. For a straight beam of the same length and bending modulus as the test beam, this longbow tension is $3.60kg$. The powerful effect of ura-zori is clear: As the brace height in units of the reverse height decreases from $h/h^{*} \approx 1.00$ to .542, the measured string tensions in units of the "longbow" string tension increase from $(7.63kg)/(3.60kg) \approx 2.12$ to $(11.34kg)/(3.60kg) \approx 3.15$. We propose a conjecture about yumi: By crafting yumi with ura-zori and then taking the brace height comparable to the reverse height, the string tension is more than *twice* that of a "flat" yumi with *no* ura-zori.

The smallest brace height in table 2, with $h/h^{*} \approx .542$ induces string tension over *three* times "longbow" tension. Why not achieve even higher string tensions by lengthening the string for even smaller brace heights? In particular, recall the "critical" configuration in figure 13, with brace height so low that the string is tangent to the beam at the tips, and the string tension is *four* times that of "longbow." In practice, configurations close to critical are difficult to sustain because their mechanical stability is very weak: The application of a small external force, such as barely pressing one tip, induces large distortions. Table 3 is a continuation of table 2 to near critical configurations, and beyond. The first three rows are data for near critical

Table 3: h/h^{*} versus F: Near critical configuations and beyond

$h\,(cm)$	h/h^{*}	$F\,(kg)$	$F/(\pi^2\mu/L^2)$
11.25	.500	11.9	33.5
10.3	.458	12.8	35.5
9.7	.431	13.5	38.6
7.7	.342	16.7	46.3
7.0	.311	18.8	52.5
6.0	.267	21.1	58.6

configurations, represented by the three squares in figure 14. The tensions expressed in units of the "longbow" tension of $3.60kg$ are $3.30, 3.60, 3.90$. The

near critical braced configurations are still symmetric about the midpoint of the beam, but as mentioned before, easily deformed by very slight manipulations. The photographs in figure 15 show what happens if you lengthen the string still further: The string wraps around the limb near one tip, and tangency is lost at the other. You can easily manipulate the braced beam, so it "snaps" into the mirror image configuration, with the string wrapped around the limb near the *other* tip. For these asymmetric braced configurations, we take the brace height to be the maximum elevation of the beam above the string, which happens at a point *off center* as is clear in figure 15. The remaining rows of table 3 tabulate string tension versus brace height in this modified sense. Notice the spectacularly large values of string tension, up to *six* times "longbow" tension. The diamonds in figure 14 correspond to the three asymmetric braced configurations.

The destabilization of the symmetric configurations and appearance of two asymmetric configurations as the brace height decreases below a threshold value is an example of what physicists call *spontaneous symmetry breaking*. Spontaneous symmetry breaking is an inherently nonlinear phenomenon. The linearized theory which is the basis of the theoretical brace height versus string tension relation (32) is not sufficient to model symmetry breaking. The proximity of the three diamonds corresponding to asymmetric braced configurations in figure 14 to the curve based on linearized theory should not be taken seriously.

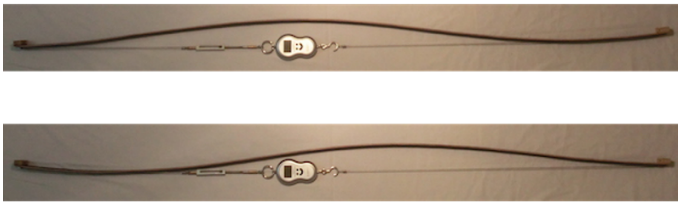

Figure 15